

CHEMISTRY

A European Journal



Accepted Article

Title: Indenoquinaldine Based Unsymmetrical Squaraine Dyes for Near-Infrared Absorption: Investigating the Steric and Electronic Effects in Dye-Sensitized Solar Cells

Authors: Nithyanandhan Jayaraj, Rajesh Bisht, and Munavvar Fairoos Mele Kavungathodi

This manuscript has been accepted after peer review and appears as an Accepted Article online prior to editing, proofing, and formal publication of the final Version of Record (VoR). This work is currently citable by using the Digital Object Identifier (DOI) given below. The VoR will be published online in Early View as soon as possible and may be different to this Accepted Article as a result of editing. Readers should obtain the VoR from the journal website shown below when it is published to ensure accuracy of information. The authors are responsible for the content of this Accepted Article.

To be cited as: *Chem. Eur. J.* 10.1002/chem.201803062

Link to VoR: <http://dx.doi.org/10.1002/chem.201803062>

Supported by
ACES

WILEY-VCH

Indenoquinaldine Based Unsymmetrical Squaraine Dyes for Near-Infrared Absorption: Investigating the Steric and Electronic Effects in Dye-Sensitized Solar Cells

Rajesh Bisht^[a, b], Munavvar Fairoos Mele Kavungathodi^[a], and Jayaraj Nithyanandhan^{[a, b]*}

Abstract: A series of near-infrared (NIR) responsive unsymmetrical squaraine dyes (**ISQ1-3**), incorporating a fused indenoquinaldine based donor, were designed and synthesized. The sp³-C center available on the indene unit of indenoquinaldine was employed to incorporate twelve-carbon alkyl chains in an out-of-plane direction to control dye aggregation on titanium dioxide (TiO₂) surface. Indole (**ISQ1**), benz[e]indole (**ISQ2**) and quinoline (**ISQ3**) moieties were included towards anchoring group to extend the absorption in NIR region and systematically study the effect of the electronic modification on DSSC performance. All the dyes exhibited intense absorption ($\epsilon \geq 10^5 \text{ M}^{-1}\text{cm}^{-1}$) in the NIR region, and dye-adsorbed TiO₂ films exhibited broad panchromatic absorption. The incident photon-to-current efficiency (IPCE) spectrum of the **ISQ3** based device displayed panchromatic IPCE response up to 880 nm. **ISQ3** sensitized device provided the best efficiency of 4.15 % with short circuit current density (J_{sc}) of 10.02 mAcm⁻², open-circuit voltage (V_{oc}) of 0.58 V and fill factor (f_f) of 72% in the presence of 10 equivalent CDCA. Electrochemical impedance spectroscopy (EIS) analysis showed attenuated charge recombination in **ISQ3** sensitized DSSC which contributes to its higher V_{oc} compared to other dyes.

Introduction

Dye-sensitized solar cells (DSSCs) have attracted considerable research attention as a promising alternative to inorganic solar cells due to their ease of fabrication, economic viability, and tunability of the various device components.^[1] The performance of DSSCs has been substantially improved due to significant advances in the key components, such as molecular sensitizers, *n*-type semiconductors, redox couples, and cathode materials in the past two decades.^[2] Sensitizing dyes play a crucial role in directing the various photovoltaic parameters which eventually affect the power conversion efficiency (PCE or η) of the DSSCs. Several sensitizers, which includes ruthenium (II) complexes,^[3] zinc-porphyrin complexes^[4] and metal-free organic dyes^[5] have

been explored. Ruthenium(II)polypyridyl complexes are among the most studied sensitizers, and PCE up to 11.5% was achieved^[3c] whereas the DSSC based upon a panchromatic porphyrin sensitizer, containing a benzothiadiazole (BTD) moiety, yielded PCE up to 13%.^[4b] Metal-free organic dyes have unique advantages over metal-organic complex based sensitizers in terms of low cost, non-toxicity, flexibility in molecular designing and tunability in electronic properties.^[5a] Several metal-free sensitizers with donor- π -acceptor (D- π -A) and donor-acceptor- π -acceptor (D-A- π -A) configuration have been explored.^[6] They show high molar extinction coefficients due to intramolecular charge transfer (ICT) which occurs within the molecule because of the push-pull effect. The efficiencies over 10% have been achieved for metal-free dyes^[7] with I⁻/I₃⁻ redox mediator whereas indenoperylene based dyes achieved PCE ≥ 12 % with Co(II/III) redox shuttle in a single sensitizer device configuration.^[8] Recently, an efficiency (PCE) of >14% was achieved by a metal-free organic dye bearing silyl anchoring group through co-sensitization.^[9]

In DSSCs, near-infrared absorbing organic dyes are critically needed as they are capable of generating high current density which can improve the performance of the cell.^[10] While there has been remarkable progress in DSSC performance of metal-free organic dyes in the last two decades, there is still ample scope for improvement in terms of dye design, especially the absorption in the near-infrared region (750-1000 nm). Squaraine dyes are among the few sensitizers which have potential to absorb in this region other than porphyrin and phthalocyanine.^[11] Squaraine dyes belong to the family of polymethine dyes and comprise of resonance-stabilized zwitterionic structures.^[12] Due to strong absorption ($\epsilon > 10^5 \text{ M}^{-1}$) in far red and NIR region, squaraine dyes have found applications in wide range of areas such as imaging,^[13] sensors,^[14] nonlinear optics,^[15] photodynamic therapy^[16], and photovoltaics.^[17] There are several successful DSSCs based on squaraine dyes which absorb in the far-red region, however, only a few of them have a spectral response over 800 nm (Figure 1). The extension of indole based core-symmetric squaraine dyes by using a π -spacer in YR6^[18] and RSQ2^[19], leads to good incident photon to current efficiency (IPCE) in NIR region (onset at 775-780 nm) with efficiency (η) of 6.7 and 6.8% respectively. The core-dissymmetric squaraine dye JK-217, assembled using thiophenyl, pyrrolyl and indolium groups, exhibits a panchromatic light harvesting up to 850 nm to yield efficiency of 5.5%.^[20] (Detailed explanation on squaraine dyes classification is provided in the supporting information, Scheme S1). In order to extend response further in the NIR region, the fused π -extended heterocyclic structures have been incorporated in

[a] R. Bisht, M.F. M. Kavungathodi, Dr. J. Nithyanandhan
Physical and Materials Chemistry Division
CSIR-National Chemical Laboratory,
Dr. Homi Bhabha Road, Pune-411008, India.
E-mail: j.nithyanandhan@ncl.res.in

[b] R. Bisht, Dr. J. Nithyanandhan
Academy of Scientific and Innovative Research (AcSIR)
New Delhi 110025, India

Supporting information for this article is given via a link at the end of the document.

squaraine dyes as they can induce strong intramolecular charge transfer (ICT) as well as maintain planarity of the molecule.

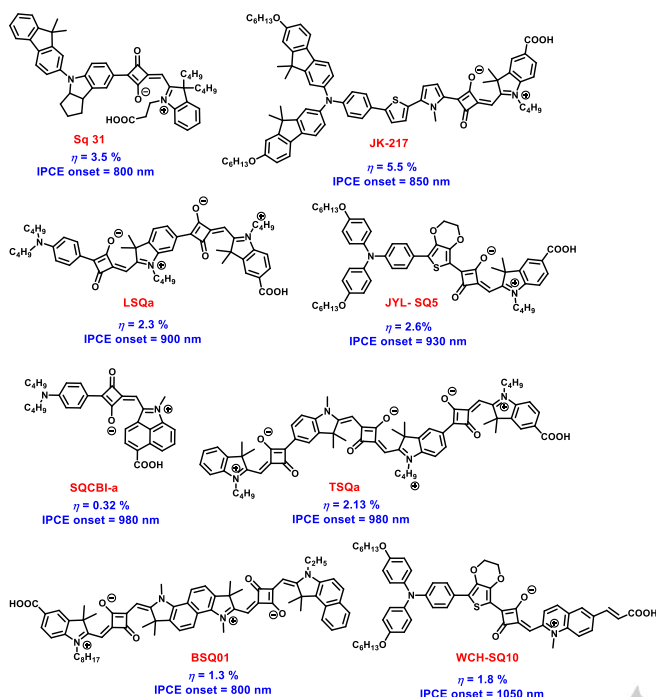


Figure 1. Examples for the best NIR responsive core-dissymmetric squaraine dyes with IPCE onset greater than 800 nm.

Pyrylium, thiopyrylium, benzo[c,d]indolenine, quinolinium and indole based heterocyclic components have been used to synthesize NIR absorbing squaraine dyes which exhibit IPCE onset at ca. 800-940 nm.^[21] The dye WCH-SQ10, consisting of triphenylamine as a donor and carboxyquinoline unit as acceptor, extends the absorption further and IPCE up to 1050 nm is obtained.^[22] In another approach, a fused dimeric squaraine dye BSQ01^[23] shows IPCE response up to 800 nm whereas the dimeric (LSQa)^[24] and trimeric (TSQa-b)^[25] squaraine dyes demonstrate improved IPCE onsets at 900 nm and 980 nm respectively. Despite the strong NIR absorption, the squaraine dyes based on fused π -extended heterocyclic structures have low efficiency (ca. 1-3 %) due to dye aggregation on TiO₂ and lack of directionality for charge injection from the photo-excited state of the sensitizer.

The aggregation of dyes on TiO₂ is a common feature in squaraine based dyes which occur due to the interaction of intermolecular dipoles.^[26] Head-to-head dipole interaction forms H-aggregates which appear as the blue-shifted peak, whereas head-to-tail dipole interaction leads to and J-aggregates which appear as red-shifted absorption compared to the absorption peak of the monomeric dye^[27]. While the aggregation of dyes on TiO₂ broadens the absorption profile, it can also reduce the charge injection into TiO₂ through exciton quenching which hampers the performance of DSSC.^[28] Thus controlling the dye

assembly on the TiO₂ is very important and the most popular method involve co-adsorption of dyes with an optically transparent substance bearing an anchoring group, such as 3 α ,7 α -dihydroxy-5 β -cholanic acid (CDCA) which help to break down the large aggregates to induce the favorable charge injection.

Incorporation of bulky alkyl chains on dye skeleton is another method to avoid aggregation in which π -stacking of molecules is restricted by increasing the bulk surrounding the chromophore.^[29] Introducing in-plane and out-of-plane alkyl groups helps controlling self-organization of dye molecules in organic photovoltaics.^[30] In DSSCs, such introduction of out-of-plane alkyl groups provides better control over aggregation at a molecular level compared to CDCA and improves device performance.^[29c,29d,31] Besides, CDCA can reduce the dye loading beyond optimal amount if used in excess, especially with highly aggregating dyes, which makes the integration of out-of-plane alkyl chains on dye preferable.

Controlling the aggregation of dyes on the TiO₂ surface has been a major challenge in NIR absorbing sensitizers. To this end, we have designed and synthesized a series of unsymmetrical squaraine dyes (**ISQ1-3**) for DSSC consisting of a fused indenoquinaldine based donor which can help in increasing the absorption in NIR region and also accommodates long alkyl chains at its sp³-C center to control dye aggregation on TiO₂ surface (Figure 2). Quinaldine is chosen to fuse with indene as it has the ability to provide excellent absorption in the NIR region in squaraine dyes.^[32] While all the dyes retain indenoquinaldine as a donor, carboxyindolenine (**ISQ1**), carboxybenzo[e]indolenine (**ISQ2**) and carboxyquinaldine (**ISQ3**) were used towards anchoring group to systematically investigate their effect on electronic properties of dyes and DSSC parameters.

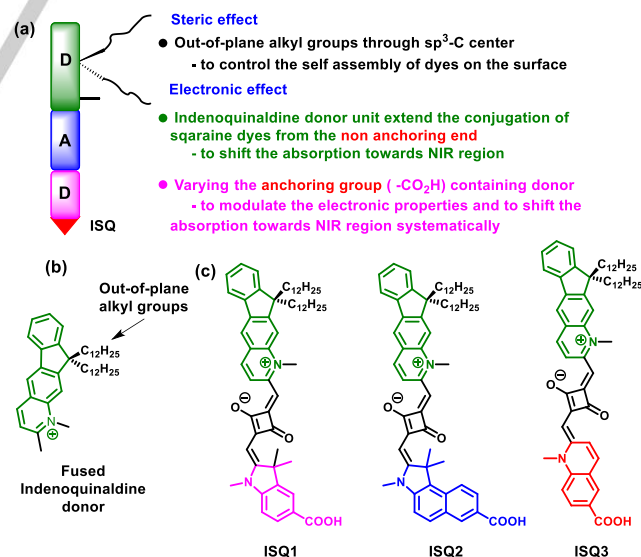
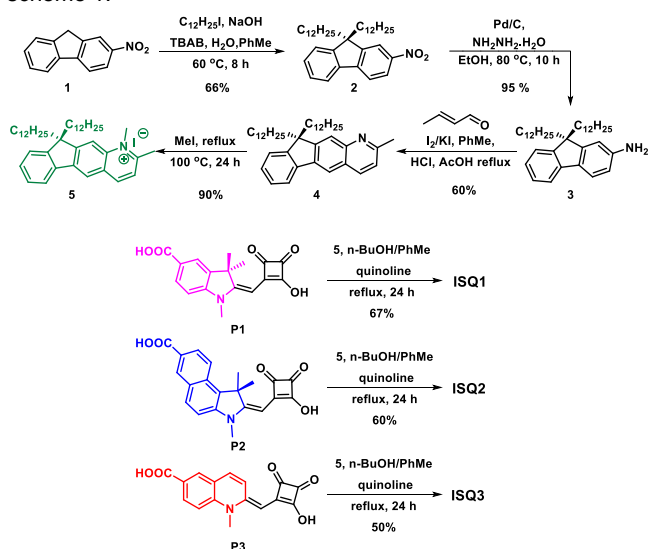


Figure 2. (a) Design of steric and electronic effects incorporated unsymmetrical squaraine dyes, (b) Structure of fused indenoquinaldine based donor and (c) Unsymmetrical squaraine dyes ISQ1-3

Results and Discussion

Synthesis

The synthetic scheme for the dyes **ISQ1-3** is illustrated in scheme 1.



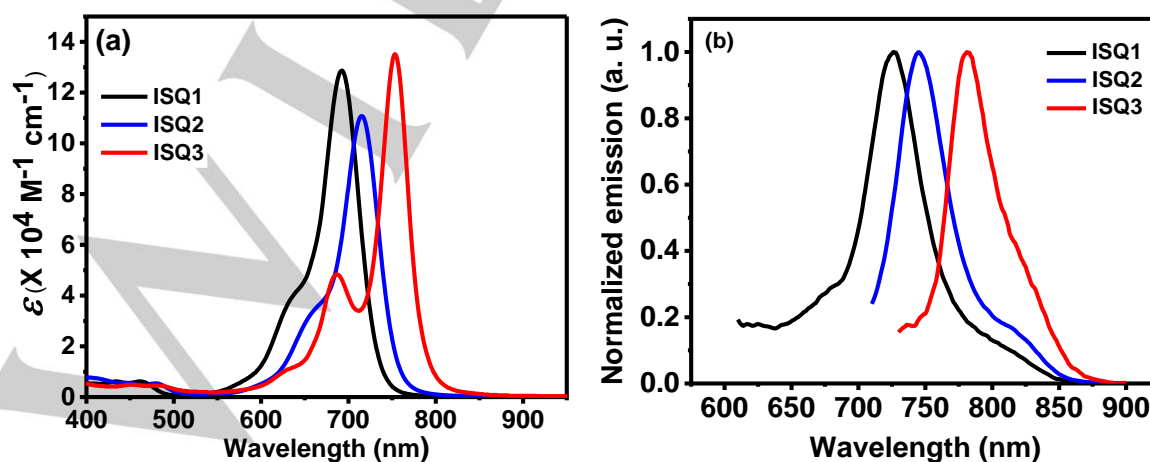
Scheme 1. Syntheses of a) indenoquinaldinium iodide **5**, (b) Indenoquinaldine donor based unsymmetrical squaraine dyes (**ISQ1-3**).

The key step in the synthetic route of **ISQ** dyes is the synthesis of indenoquinaldinium salt **5**, which begins with functionalization of 2-nitrofluorene (**1**) with 12 carbon long chains by treatment with NaOH in the presence of dodecyl iodide. The resultant compound **2** was reduced to 2-amino-9,9-didodecylfluorene (**3**) by hydrazine hydrate in the presence of catalyst Pd/C. The amine derivative **3** was treated with crotonaldehyde under Skraup-Doebner-Von Miller reaction condition to afford indenoquinaldine derivative **4** which was subsequently reacted with iodomethane to give N-methyl indenoquinaldinium salt **5**. The synthesis of semi-squaric acid derivatives of carboxyindole **P1**, carboxybenz[e]indole **P2**, and carboxyquinoline **P3** is

described in supporting information (Scheme S2). In the final step, the semi-squaric acid derivative **P1** was refluxed with indenoquinaldinium salt **5** in *n*-BuOH/PhMe mixture under azeotropic distillation of water employing Dean–Stark apparatus to give squaraine dyes **ISQ1**. Similarly, the dyes **ISQ2** and **ISQ3** were obtained by treating **5** with **P2** and **P3** respectively. All the dyes were thoroughly characterized by ¹H-NMR, ¹³C-NMR spectroscopy, and mass spectrometric techniques.

Optical characterization

To evaluate the optical properties of dyes, UV-Vis absorption and emission spectra of **ISQ1-3** were recorded in CHCl₃ solutions (Figure 3) and data are summarized in (Table 1). **ISQ** dyes exhibited intense absorption bands in the far-red region with high extinction coefficient ($\geq 10^5$ M⁻¹cm⁻¹) due to strong intramolecular charge transfer (ICT) process. **ISQ1** showed the absorption maximum (λ_{max}) at 692 nm with onset at 734 nm due to the strong donating effect of the indenoquinaldine unit. The red-shifted λ_{max} at 715 nm with onset at 760 nm was observed for **ISQ2** due to additional conjugation by carboxybenz[e]indole unit towards anchoring group. In **ISQ3**, due to the presence of quinaldine moiety on both ends of central squaraine unit, the maximum bathochromic shift was observed, and λ_{max} was determined at 754 nm with onset at 800 nm (Figure 3a). The same trend was observed in the emission spectra of the dyes which displayed emission maxima at 726 nm, 745 nm and 781 nm for **ISQ1**, **ISQ2** and **ISQ3** respectively (Figure 3b). The band gap (E_{0-0}) was obtained from the intersection of absorption and emission curve and found to be at 1.75 eV, 1.70 eV and 1.62 eV for **ISQ1**, **ISQ2**, and **ISQ3** respectively. Apart from the intense absorption in NIR region, a weak absorption ($\epsilon \approx 10^3$ M⁻¹cm⁻¹) in the visible region was observed between 400 to 500 nm for **ISQ1-3** which can be beneficial to absorb the high energy photons as well. To understand the self-assembly of dyes on TiO₂ film, the titania coated glass was immersed in a 0.1 mM dye solution for 15 minutes. Exposing the TiO₂ film to the dyes for short duration also gives information about the self-organization of dyes on the TiO₂ surface.



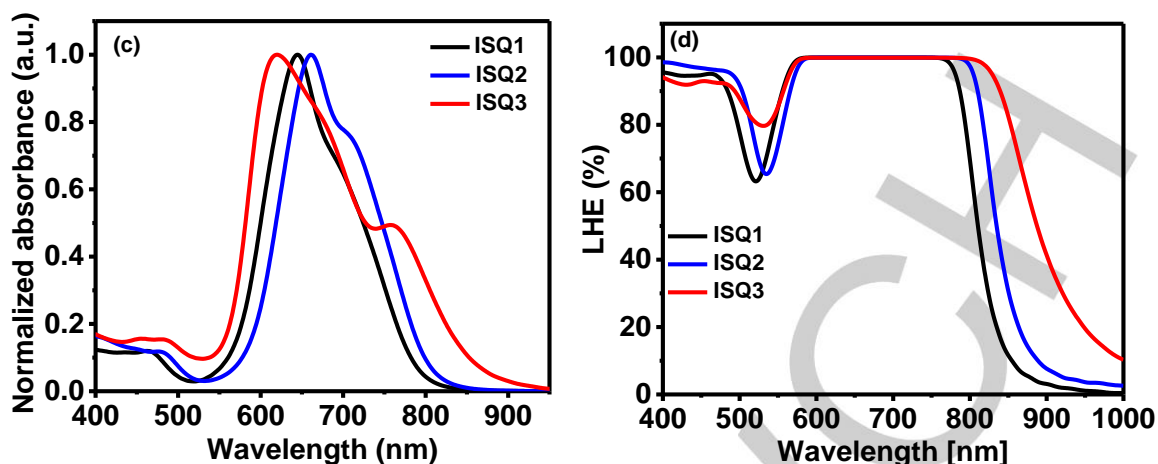


Figure 3. a) The absorption spectra of **ISQ1-3** in CHCl_3 ([dye] = 6 μM), (b) Normalized emission spectra ([dye] = 6 μM in CHCl_3 , λ_{exc} = 600 nm (**ISQ1**), 700 nm (**ISQ2**) and 720 nm (**ISQ3**), (c) Normalized absorption spectra of **ISQ** dyes immobilized on TiO_2 , and (d) Light harvesting efficiency of the **ISQ** dyes.

The absorption spectra of dye anchored on TiO_2 film displayed large spectral broadening compared to the spectra in solution due to the interaction of anchoring group (-COOH) with TiO_2 ,^[33] and the formation of H-type (blue-shifted) aggregates predominantly^[34] (Figure 3c). The formation of aggregates were confirmed by comparing the absorption spectra of dyes on TiO_2 in the absence and the presence of CDCA (Figure S2). Addition of CDCA leads to a decrease in the extent of H-aggregate with a concomitant increment of monomeric dyes on the surface. All the dyes indicated the extensive formation of H-aggregates with blue-shifted peaks of high-intensity observed at 645, 661 and 620 nm for **ISQ1**, **ISQ2** and **ISQ3** respectively. The shoulder peaks were also observed at 693, 714 and 753 nm for **ISQ1**, **ISQ2**, and **ISQ3** nm respectively, which belongs to the absorption by monomers. **ISQ3** exhibited maximum peak broadening with absorption ranging from 550 nm to 900 nm. The light harvesting efficiency ($\text{LHE} = 1-10^{-A}$) was calculated by measuring absorption in transmittance mode of dye adsorbed films which was obtained by immersing the TiO_2 film in the dye solution for a long period of 6 h (Figure 3d). The LHE of dyes anchored on TiO_2 indicates the ability of dyes to absorb the fraction of photons of different energy across the solar spectrum. LHE profiles showed that **ISQ1-3** dyes are able to harvest the photons from visible as well as NIR region with $\text{LHE} \geq 90\%$ in 400-500 nm and 550-850 nm range, which makes these sensitizers suitable candidates for panchromatic absorption. The dyes **ISQ1**, **ISQ2**, and **ISQ3** showed LHE onset at 850 nm, 880 nm, and 1000 nm respectively which lie well in the NIR region.

Electrochemical characterization

Cyclic voltammetry was carried out in CH_2Cl_2 solutions to evaluate the redox properties of the dyes in order to determine the feasibility of charge injection from the excited dye into the

conduction band of the TiO_2 and the dye regeneration by the electrolyte (Figure 4).

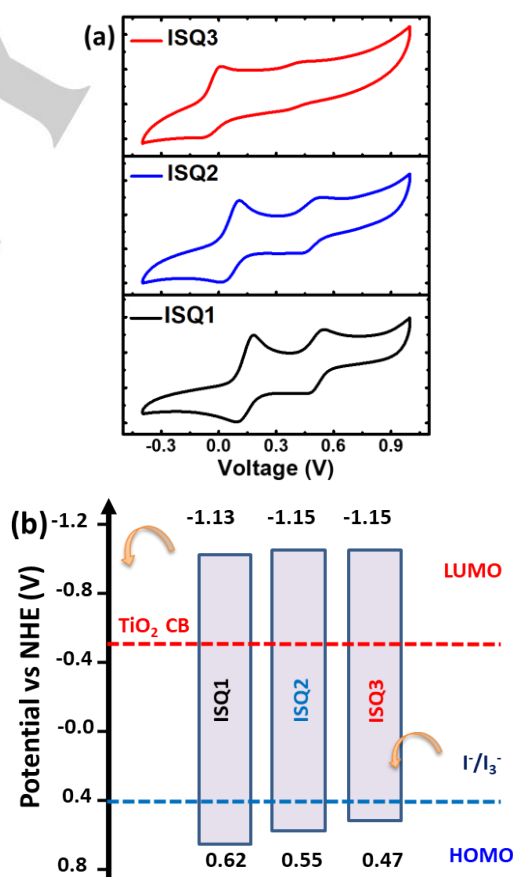


Figure 4. (a) Cyclic voltammogram of **ISQ** dyes measured in CH_2Cl_2 (b) Energy level diagram for **ISQ** dyes with DSSC device components.

Table 1. Optical and electrochemical properties of ISQ dyes

Dyes	$\text{abs}\lambda_{\text{max}}/\text{CH}_2\text{Cl}_2$ (nm) ^a	$\text{eml}\lambda_{\text{max}}/\text{CH}_2\text{Cl}_2$ (nm) ^b	$\text{abs}\lambda_{\text{max}}/\text{TiO}_2$ (nm) ^c	$\epsilon \times 10^4$ ($\text{M}^{-1}\text{cm}^{-1}$) ^d	E_g^{DFT} (eV) ^e	E_{HOMO} (V vs NHE) ^f	E_{0-0}^{opt} (eV) ^g	E_{LUMO} (V vs NHE) ^h
ISQ1	462, 692	726	645, 693	0.62, 12.9	2.09	0.62	1.75	-1.13
ISQ2	480, 715	745	661, 714	0.56, 11.1	1.97	0.55	1.70	-1.15
ISQ3	487, 754	781	620, 682, 753	0.43, 13.5	1.77	0.47	1.62	-1.15

^aSee SI for experimental details of measurements and calculations

HOMO levels of the dyes **ISQ1-3** were obtained from the first oxidation onset and calculated to be at 0.62 V, 0.55V, and 0.47 V respectively (Vs. NHE). The upward shift of HOMO in case of **ISQ2** and **ISQ3** can be credited to the stronger donating effect of benz[e]indole and quinoline respectively compared to indole. **ISQ1** shows high potential offset ($-\Delta G_{\text{reg}} = 220$ mV) with respect to redox level of I^-/I_3^- (0.4 V) which provides large driving force for effective dye regeneration whereas **ISQ2** ($-\Delta G_{\text{reg}} = 150$ mV) and **ISQ3** ($-\Delta G_{\text{reg}} = 70$ mV) shows moderate driving force (Figure 4b). The LUMO levels were calculated by subtracting E_{0-0} from E_{HOMO} and found to be at -1.13 V, -1.15 V and -1.15 V (vs NHE) for ISQ1, ISQ2, and ISQ3 respectively which gives enough energy offset ($-\Delta G_{\text{inject}} \approx 700$ mV) for charge injection on conduction band (CB) of TiO_2 (-0.5 V). While the HOMO levels varied significantly, the LUMO levels were essentially the same for all the dyes.

Computational studies

To deeply understand the structural, electronic, and optical properties of **ISQ** dyes, quantum mechanical calculation were carried out using density functional theory (DFT) and time-dependent DFT (TD-DFT) at B3LYP/6-31G (d,p) level in Gaussian 09.^[35] Suitable spatial distributions of the frontier molecular orbitals (FMO) are crucial for facilitating the electron-transfer processes. Ideally, the highest occupied molecular orbitals (HOMO) should be away from the TiO_2 , and lowest unoccupied molecular orbitals (LUMO) should be as close as possible to the TiO_2 for efficient electron injection. Isodensity surface plots of **ISQ1-3** dyes show that HOMO are predominantly confined over central squaric acid units (Figure 5).

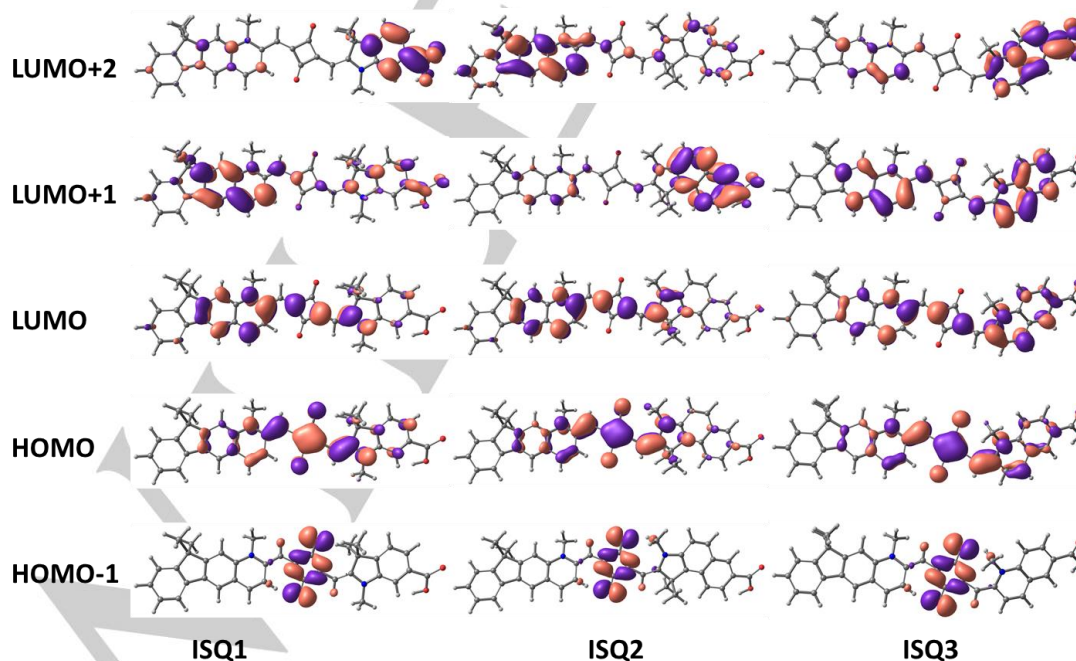


Figure 5. Isodensity surface plots of **ISQ1-3** dyes (alkyl chains are removed for clarity).

The HOMO and LUMO overlap for the most part of **ISQ1-3** dyes, however, there is slight delocalization of LUMO towards the anchoring group in case of **ISQ3** LUMO+1 and LUMO+2 are prominently delocalized towards anchoring group for the **ISQ3** dye which suggests that it can exhibit better charge injection compared to **ISQ1-2** and can counterbalance the effect of low driving force for dye regeneration. Simulated absorption spectra were plotted using TD-DFT (Figure S1), and spectra were found to be consistent with the experimental spectra. By comparing the two spectra it can be predicted that the peaks of high oscillator strength at longer wavelength originates exclusively from HOMO-LUMO vertical energy transition (> 99 % contribution) in all the dyes whereas the high energy peaks with low oscillator strength between 350 and 500 nm are associated with the transition to higher excited states, i.e., LUMO+1, LUMO+2 (Table S1). The optimized geometry in Figure 6 shows that the distance between branched alkyl chains and oxygen atoms of anchoring unit **d** is about 20.5 Å, 22.Å and 19.8 Å for **ISQ1**, **ISQ2**, and **ISQ3** respectively.

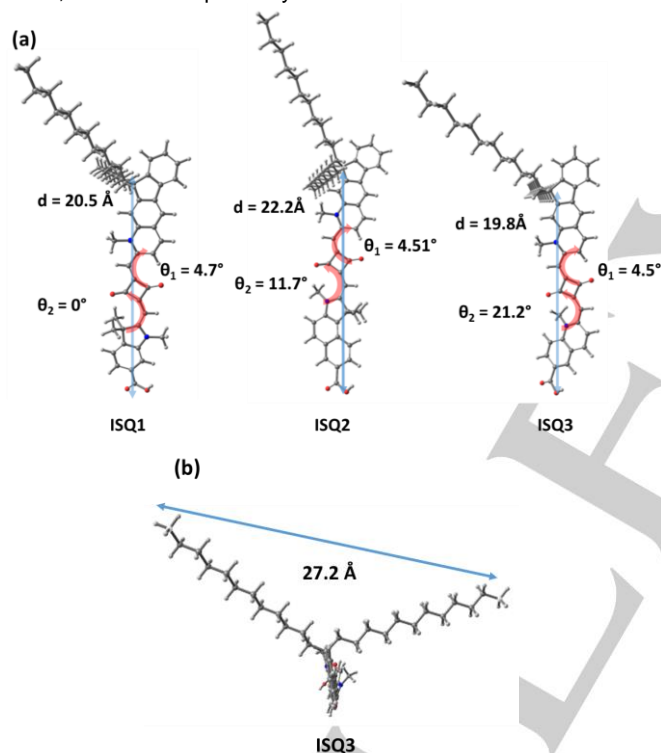


Figure 6. Optimized geometry of **ISQ1-3** dyes, a) Lateral view, b) Top view

The dihedral angle between indenoquinoline and squaraine unit (θ_1) is the same for all the dyes whereas the dihedral angle between squaraine units and anchoring unit is different for all the dyes. The dye **ISQ1** is almost planar with $\theta_1 = 4.5^\circ$ and $\theta_2 = 0^\circ$, **ISQ2** is non-planar with $\theta_2 = 11.7^\circ$, and planarity is further reduced in **ISQ3** with $\theta_2 = 21.2^\circ$. The distance between the terminal carbons of the two out of plane alkyl chains on the dyes is about 27 Å which helps in controlling the dye-dye interactions on the TiO_2 surface (Figure 6b).

Photovoltaic characterization

The photovoltaic measurements of the DSSCs fabricated using **ISQ1-3** dyes were done under irradiance of 100 mWcm^{-2} simulated AM 1.5G sunlight. The current density-voltage (J-V) plot and IPCE spectra of the best cells are shown in Figure 7 and summarized in table 1. The DSSC based on **ISQ1** gave the PCE of 3.24 % whereas **ISQ2** and **ISQ3** showed PCE of 2.35 % and 1.85% respectively, without using any co-adsorbent. The major difference in their performance comes from the variation in the short circuit current density (J_{SC}) which is highest for **ISQ1** (8.99 mAcm^{-2}), followed by **ISQ2** (6.85 mA cm^{-2}) and **ISQ3** (5.23 mA cm^{-2}). The low short circuit current density could be ascribed to the strong aggregation of dye on TiO_2 which is maximum in case of **ISQ3**. To minimize the negative effect of aggregation on cell performance, the dye was co-adsorbed in the presence of CDCA to reduce the self-quenching of excitons and charge recombination. All the **ISQ** dyes showed a different response with the addition of CDCA. The efficiency of **ISQ1** dyes reduced to 2.63 % mainly due to a reduction in J_{SC} (6.86 mA cm^{-2}), even though the slight improvement in V_{OC} was observed (0.558 V). In contrast, the performance of **ISQ2** and **ISQ3** sensitized cells improved when co-adsorbed with CDCA. **ISQ2** achieved the maximum efficiency of 3.68% on addition of 5 equiv CDCA with V_{OC} of 0.558 V and J_{SC} of 9.62 mA cm^{-2} whereas **ISQ3** reached the best efficiency of 4.15% with J_{SC} of 10.02 mA cm^{-2} , V_{OC} of 0.576 V, and ff of 72%, in presence 10 equiv of CDCA. Further addition of CDCA led to a reduction in device efficiency of all the dyes, primarily due to substantial loss of J_{SC} (Figure S3 and Table S2). It was suspected that the decrease in efficiency of **ISQ1** on the addition of CDCA could be due to reduced adsorption of dyes on the TiO_2 surface due to competitive binding of CDCA. To confirm our hypothesis, the dye loading was calculated by desorption of dye-sensitized photo-anodes in the presence of 2M ethanolic HCl followed by spectrophotometric measurement of dye concentration (Table 2). In the case of **ISQ1**, the addition of CDCA, as low as 5 equivalents, led to the drastic decrease of 68% in dye content. The dye loading of **ISQ2** with 5 equiv of CDCA (1.22×10^{-7} mol cm^{-2}) was significantly higher than the dye content of **ISQ1** devices with 5 equiv. CDCA (7.56×10^{-8} mol cm^{-2}). **ISQ3** sensitized cells, even in the presence of 10 equiv CDCA, showed higher dye content (1.05×10^{-7} mol cm^{-2}) compared to **ISQ1** (5 equiv CDCA). This shows that dye- TiO_2 interaction is poor in case of **ISQ1** which allows the dyes to be replaced by CDCA on TiO_2 rather easily compared to **ISQ2** and **ISQ3** (Figure 8b (ii)).

Thus, the variable effect of CDCA on performance of DSSC could be ascribed to competitive binding of **ISQ1-3** dyes with CDCA, where on the one hand CDCA helps in improving J_{SC} and V_{OC} by reducing exciton quenching induced by aggregation on TiO_2 surface, on the other hand, it may replace the dye molecules to reduce the effective dye content on the photo-anode leading to poor performance.^[19]

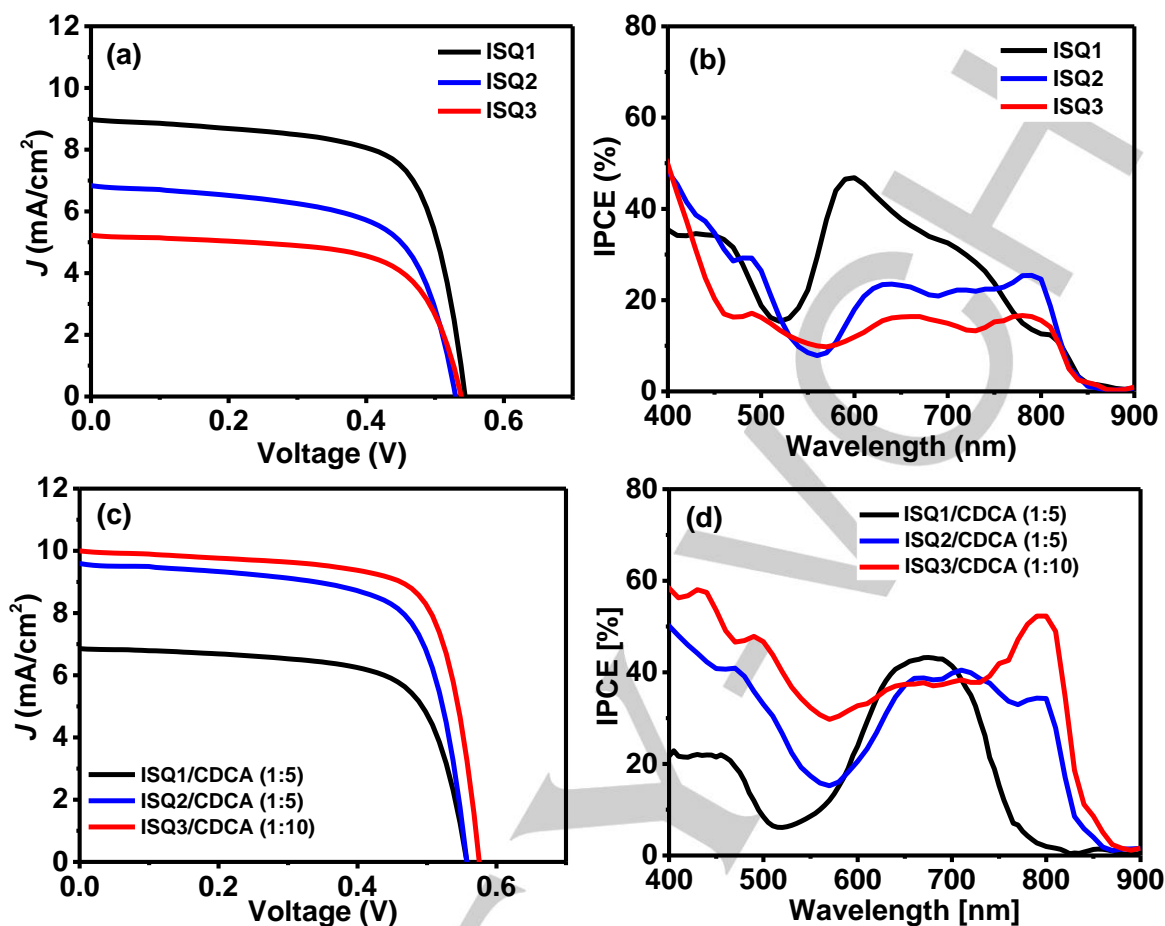


Figure 7. J - V and IPCE characterization of ISQ dyes. (a, b) J - V and IPCE curves for ISQ1-3 in the absence of CDCA. (c, d) J - V and IPCE curves for ISQ1-3 in the presence of CDCA.

Table 2. Photovoltaic parameters for DSSCs employing the I^-/I_3^- electrolyte under the optimized conditions^a

Dyes	J_{sc} (mA cm^{-2})	$\text{INT } J_{sc}^b$ (mA cm^{-2})	V_{oc} (V)	ff (%)	η (%)	Dye loading ^c (mol cm^{-2})
ISQ1	8.99	8.46	0.544	68.4	3.34	2.33×10^{-7}
ISQ1/CDCA(1:5)	6.86	6.23	0.558	68.9	2.63	7.56×10^{-8}
ISQ2	6.85	6.52	0.537	64.1	2.35	2.82×10^{-7}
ISQ2/CDCA (1:5)	9.62	9.37	0.558	68.7	3.68	1.22×10^{-7}
ISQ3	5.23	4.93	0.538	65.7	1.85	2.54×10^{-7}
ISQ3/CDCA (1:10)	10.02	11.16	0.576	72.0	4.15	1.05×10^{-7}

^aSee SI for experimental details of measurements and calculations. ^bCalculated by integrating IPCE over the standard AM1.5G emission spectrum (ASTM G173-03).

The variation in J_{SC} can be further explained through a detailed investigation of IPCE spectra as the J_{SC} is directly related to IPCE and can be expressed as eq 1, where q is the charge of the electron, and ϕ is the photon flux of solar spectrum (AM 1.5 G).

$$J_{SC} = q \int IPCE(\lambda) \phi(\lambda) d\lambda \quad (1)$$

In the absence of CDCA, **ISQ1** showed best IPCE response with a maximum of 46% at 600 nm which is primarily contributed by the H-type aggregates (Figure 6b). The peak with low IPCE (12%) at 810 nm can be attributed to current generation from J-aggregates. When CDCA is added, the aggregation was reduced effectively which can be observed as the disappearance of the peaks at 600 nm and 810 nm (Figure 6d). The reduction in aggregation, though improved the V_{OC} from 0.544V to 0.558 V in **ISQ1** based cell, the severe decrease in dye amount led to low IPCE which in turn led to reduced J_{SC} . In the case of **ISQ2**, the H-aggregates (23 % at 640 nm) and J-aggregates (25 % at 790 nm) contributed almost equally to IPCE, however, the overall response was much lower compared to **ISQ1**. Similarly, for **ISQ3** the IPCE response was quite low with equal contribution from H- (16 % at 660 nm) and J- aggregates (16 % at 780 nm). The reason behind the low IPCE for **ISQ2** and **ISQ3**, in the absence of CDCA, could be the formation of closely stacked large-sized aggregates which could not inject an electron into the TiO_2 (Figure 8a). The extended π -surface of **ISQ2** and **ISQ3** due to benz[e]indole and quinoline moieties respectively may induce such close intermolecular packing, and the absence of out-of-plane two methyl group on carboxyquinoline group may cause the **ISQ3** to be aggregate excessively. When CDCA was added, both **ISQ2** and **ISQ3** showed improved IPCE response. **ISQ2** (5 equiv CDCA) showed IPCE of over 30% in between 650 to 800 nm with three

distinct humps on the curve which are contributed by the H-type aggregates (39 % at 650 nm), monomers (40 % at 710 nm) and J-type aggregates (34 % at 800 nm). In the case of **ISQ3** (10 equiv CDCA), the contribution by J- aggregates was more prominent with IPCE over 50% at 800 nm whereas IPCE of 30-40 % was obtained in the range of 600-750 nm which was contributed mainly by the monomers, dimers and H-type dye aggregates on the TiO_2 surface. The results indicate that for **ISQ2** and **ISQ3**, the addition of CDCA facilitated the formation of smaller aggregates in a controlled fashion which helped to inject electron more efficiently while maintaining the broad spectrum in comparison to the devices without CDCA (Figure 8b (ii)). Remarkably, a substantial IPCE response of over 40 % in the visible region (400-550 nm) was also observed for **ISQ3**. The origin of this response can be traced to the high concentration of electron density on anchoring group in higher excited states (LUMO, LUMO+1, and LUMO+2) which led to strong electronic coupling and good charge injection into the TiO_2 despite low oscillator strength. Hence, with the help of panchromatic IPCE, **ISQ3** attained better J_{SC} compared to other dyes and eventually higher efficiency.

Though **ISQ** dyes have similar indenoquinoline based donor on the non-anchoring side, the anchoring unit containing different donor units plays a vital role in determining the stability of the monolayer thus formed on the TiO_2 surface. For example, the nature of IPCE profile of **ISQ3** was almost similar with and without CDCA indicating the contribution from monomers, H- and J-aggregates (Figure S3(f)). Whereas for **ISQ2**, the IPCE profile showed the contribution from monomers, H- and J-aggregates up to 5 equiv. of CDCA, and further addition of CDCA leads to contribution mainly from monomers and dimers (Figure S3(d)). In the case of **ISQ1**, without CDCA, the obtained photocurrent is due to both monomer and aggregates (H- and J-).

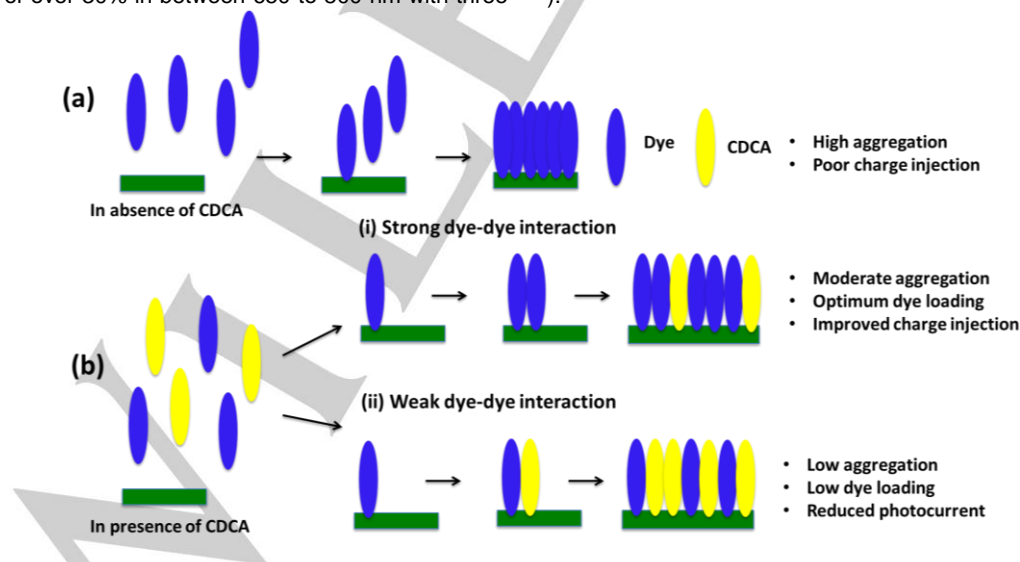


Figure 8. Cartoon representation of the formation of dye aggregate and variation in dye loading in the (a) absence of CDCA and the (b) presence of CDCA.

Addition of 5 equiv of CDCA disturbed the self-assembly of **ISQ1**, and consequently, the photocurrent is derived mainly from monomer and dimer (Figure S3(b)). Hence the nature of the anchoring unit containing donor units not only modulate the electronic property of **ISQ** dyes but also controls the self-assembly of dyes on the TiO_2 surface.

Electrochemical Impedance Spectroscopy (EIS).

To understand the slight difference in V_{OC} values of **ISQ** sensitized cell electrochemical impedance spectroscopy (EIS) was carried out under dark conditions. Referring to the energy band diagram and the carrier transfer processes in Figure 4, the V_{OC} is calculated from the potential difference between the quasi-Fermi level of TiO_2 (E_F) and the chemical potential of redox species (E_{redox}) in an electrolyte (eq2).^[36]

$$V_{OC} = E_{redox} - E_F \quad (2)$$

$$E_F = E_{CB} + k_B T \ln(n_c/N_c) \quad (3)$$

According to eq 3, the variation in E_F is linked to the number of electrons on the TiO_2 (n_c) and conduction band (E_{CB}) of TiO_2 , where k is Boltzmann constant, N_c is the effective density of state, and T is the absolute temperature (293 K). Thus, V_{OC} is intimately susceptible to shift in the TiO_2 conduction band edge (E_{CB}), which can be deduced from the chemical capacitance (C_μ) and fluctuation of electron density, which is associated to the electron lifetime(s) determined by the charge recombination rate.^[37] Typical EIS Nyquist plots for DSSCs based on the **ISQ1-3** dyes were measured in the dark under applied bias -0.5 , -0.47 , -0.44 and -0.41 V and are fitted using $R_S + R_{pt}/C_{pt} + R_{ct}/C_\mu$ circuit model (Figure 9). The larger semicircle at lower frequencies in Nyquist plots represents the interfacial charge-transfer resistance (R_{ct}) at the TiO_2 -dye/electrolyte interface.

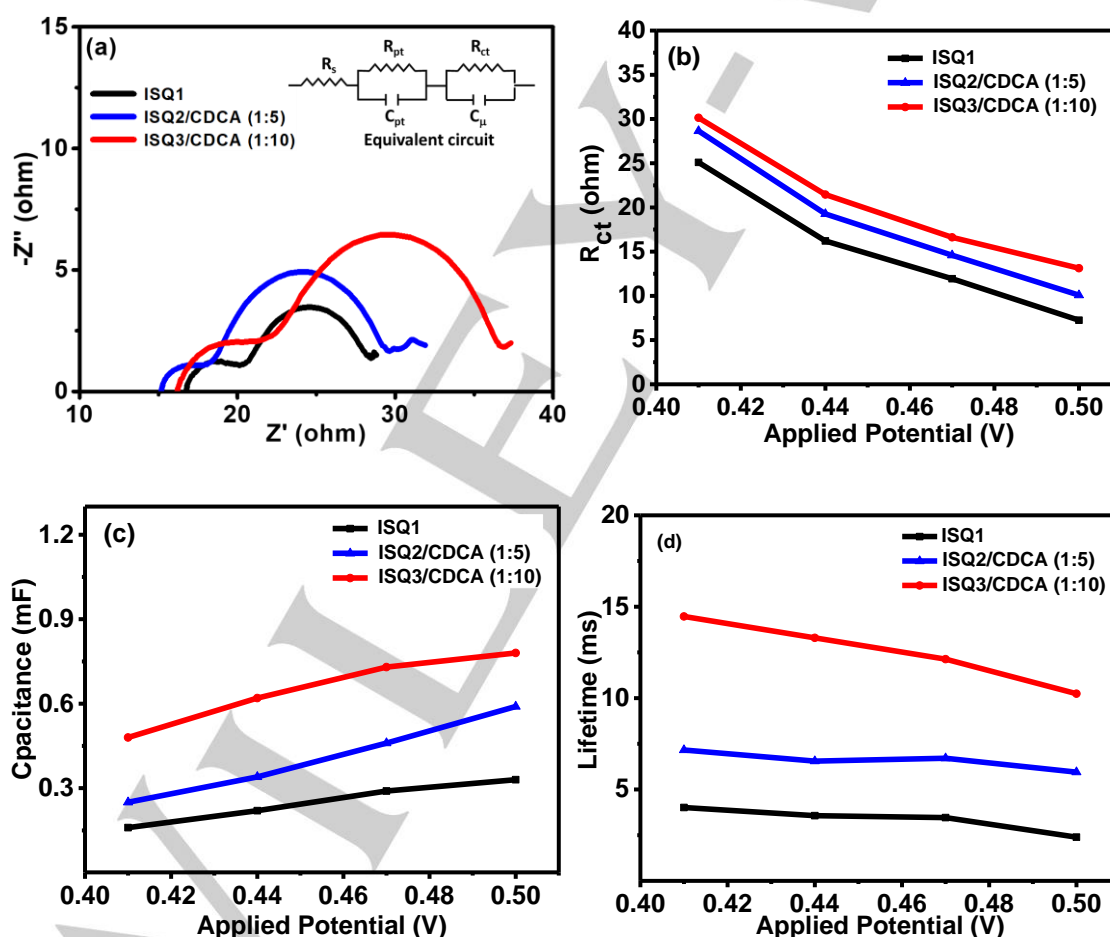


Figure 9. (a) The Nyquist plot at an applied bias of 0.5 V, (b) Charge transfer resistance (R_{ct}), (b) R_{ct} vs. applied potential, (c) C_μ vs. applied potential, and (d) τ vs. applied potential.

The fitted recombination resistance (R_{ct}) value of ISQ sensitized devices (under an applied bias of -0.5 V) increases in the order of **ISQ1** (7.25Ω) < **ISQ2** (10.08Ω) < **ISQ3** (13.13Ω), which is consistent with the sequence of V_{OC} values (Figure 8b and Table 3). Larger the R_{ct} value, slower is the recombination of electrons from the conduction band of TiO_2 to the oxidized I_3^- species in the electrolyte. The electron lifetime(s) on TiO_2 were calculated from R_{ct} and chemical capacitance C_{μ} using $\tau = R_{ct} \times C_{\mu}$. The longer electron lifetime in ISQ3 sensitized cell further supports the higher V_{OC} for **ISQ3** (10.24 ms) compared to **ISQ1** (2.39 ms) and **ISQ2** (5.94 ms) based cells (Figure 9d and Table 3).

Table 3. EIS Parameters of ISQ Dye Cells at an Applied Potential of -0.5 V in the Dark.

ISQ Dyes	R_s (ohm)	R_{ct} (ohm)	C_{μ} (mF)	τ (ms)
ISQ1	15.80	7.25	0.33	2.39
ISQ2/CDCA 5 eqv	14.56	10.08	0.59	5.94
ISQ3/CDCA 10 eqv	14.41	13.13	0.78	10.24

Conclusions

To address the dearth of efficient NIR absorbing metal-free dyes in DSSC, a series of unsymmetrical squaraine dyes (**ISQ1-3**) featuring a fused indenoquinoline as a π -extended donor have been successfully designed and synthesized. All the dyes exhibit intense absorption in the NIR region with onset at 820 nm for **ISQ3** and spectra broadened after absorption on TiO_2 surface which extends up to 1000 nm. The variable photovoltaic response was observed after the addition of CDCA where the efficiency of **ISQ1** dyes decreased in contrast to improvement in efficiency of **ISQ2** and **ISQ3** due to competitive binding of CDCA against the dye. The best devices of **ISQ2** and **ISQ3** dyes displayed panchromatic IPCE response which ranges from 400 nm to 880 nm and efficient electron injection by the both H-type and J-type aggregates along with the monomers was also observed. DFT and TDFT suggested the delocalization of LUMO+1 and LUMO+2 towards anchoring group which facilitated charge injection by high energy excitations as well especially for **ISQ3**. As a result, ISQ3 displayed the best photovoltaic properties among the dyes in the presence of 10 equiv CDCA with J_{SC} of 10.02 mAcm^{-2} , V_{OC} of 0.58 V and ff of 72% which led to the PCE of 4.15%. The results present an effective approach for developing efficient and NIR responsive sensitizers for DSSC application.

Experimental Section

Details on the reagents, equipments utilized to characterize the synthesized precursors, final dye molecules and evaluating the Photophysical, electrochemical, photovoltaics parameters, electrochemical impedance spectroscopy and procedure for the DSSC device fabrication is provided in the supporting information.

Synthetic procedure

9,9-Didodecyl-2-nitro-9H-fluorene (2). 2-Nitrofluorene (3.0 g, 14.20 mmol), 1-iodododecane (12.6 g, 42.61 mmol) and tetrabutyl ammonium bromide (0.3 g, 0.710 mmol) were taken in 70 mL toluene in two-necked round bottom flask. An aqueous solution of NaOH (23 mL, 50 % in weight) was added to the mixture rapidly with constant stirring. The resultant mixture was stirred at 60 °C for 8 h under argon atmosphere. Reaction mixture was cooled to room temperature and 1 M HCl (100 mL) was added to it followed by addition of water (100 mL). The reaction mixture was extracted with ethyl acetate, washed with brine and dried over anhydrous sodium sulphate. Solvents were removed under reduced pressure and the residue was purified by column chromatography (EtOAc-pet ether) to afford pure compound **2** as pale yellow oil (5.13 g, 66 %). $^1\text{H NMR}$ (500 MHz, CDCl_3) δ 8.26 (dd, $J = 8.3, 2.0$ Hz, 1H), 8.20 (d, $J = 2.0$ Hz, 1H), 7.83 – 7.75 (m, 2H), 7.45 – 7.36 (m, 3H), 2.08 – 1.96 (m, 4H), 1.27 – 1.12 (m, 24H), 1.08 – 1.00 (m, 12H), 0.86 (t, $J = 7.0$ Hz, 6H), 0.68 – 0.46 (m, 4H). $^{13}\text{C NMR}$ (125 MHz, CDCl_3) δ 152.5, 152.1, 147.8, 147.3, 138.9, 129.4, 127.5, 123.4, 123.436, 121.3, 119.9, 118.4, 77.2, 55.8, 40.2, 32.0, 30.0, 29.7, 29.7, 29.6, 29.5, 29.4, 23.9, 22.8, 14.3. HRMS (ESI) m/z : $[M+H]^+$ Calcd for $\text{C}_{37}\text{H}_{58}\text{NO}_2$ 548.4468, found 548.4456.

2-Amino-9,9-didodecylfluorene (3): To a mixture of compound **2** (2.0 g, 3.65 mmol) in 30 mL of EtOH, 0.2 g of 10% Pd/C was added. The resultant mixture was stirred at room temperature under argon atmosphere for 15 min. Hydrazine monohydrate (1 mL) was added dropwise over 15 min. The reaction mixture was stirred at 80 °C for 10 h. The reaction mixture was cooled to the room temperature after the completion and filtered over celite pad to collect the filtrate. The solvents were removed to give the desired compound **3** as white solid (1.8 g, 95 %). m.p. 55-57 °C. $^1\text{H NMR}$ (400 MHz, CDCl_3) δ 7.54 (d, $J = 7.5$ Hz, 1H), 7.47 (d, $J = 8.4$ Hz, 1H), 7.27 – 7.22 (m, 2H), 7.18 (d, $J = 7.2$ Hz, 1H), 6.69 – 6.62 (m, 2H), 1.97 – 1.79 (m, 4H), 1.28 – 1.14 (m, 24H), 1.10 – 1.01 (m, 12H), 0.87 (t, $J = 6.8$ Hz, 6H), 0.69 – 0.55 (m, 4H). $^{13}\text{C NMR}$ (100 MHz, CDCl_3) δ 152.8, 149.9, 146.0, 141.7, 132.7, 126.7, 125.5, 122.7, 120.6, 118.4, 114.1, 110.0, 77.2, 54.9, 40.8, 32.1, 30.3, 29.8, 29.5, 23.9, 22.8, 14.3. HRMS (ESI) m/z : $[M+H]^+$ Calcd for $\text{C}_{37}\text{H}_{60}\text{N}$ 518.4726, found 518.4718.

10,10-Didodecyl-2-methyl-10H-indeno[1,2-g]quinoline (4). In a two-necked round bottom flask, compound **3** (1.9 g, 3.60 mmol), acetic acid (0.2 mL, 3.6 mmol) and 20 mL HCl (6 M) were added. The mixture was refluxed at 100 °C for 1 h, followed by addition of iodine (42 mg, 0.18 mmol), potassium iodide (60 mg, 0.36 mmol) and PhMe (4 mL). Crotonaldehyde (0.6 mL, 7.2 mmol) was dissolved in PhMe (2 mL) and added to the reaction flask dropwise over 30 min. The resulting mixture was refluxed for another 6 h and cooled to the room temperature after completion of the reaction. The ammonia solution 10 mL was added to neutralize the reaction. 50 mL water was added to the reaction mixture, extracted by ethyl acetate and organic phase was dried over sodium sulphate. The solvents were removed under reduced pressure and the residue was purified by column chromatography (EtOAc-Pet ether) to afford pure compound **4** as dark brown oil (1.23 g, 60 %). $^1\text{H NMR}$ (400 MHz, CDCl_3) δ 8.11 (d, $J = 8.4$ Hz, 1H), 8.01 (s, 1H), 7.95 (s, 1H), 7.82 (d, $J = 4.5$ Hz, 1H), 7.41 – 7.33 (m, 3H), 7.27 (d, $J = 8.5$ Hz, 1H), 2.76 (s, 3H), 2.13 – 1.97 (m, 4H), 1.25 – 1.07 (m, 23H), 1.07 – 0.98 (m, 12H),

0.85 (t, $J = 6.9$ Hz, 6H), 0.68 – 0.58 (m, 4H). ^{13}C NMR (100 MHz, CDCl_3) δ 158.3, 153.4, 151.4, 148.2, 140.2, 140.0, 136.5, 128.3, 127.2, 126.3, 123.3, 122.2, 121.5, 120.5, 117.0, 55.2, 41.4, 32.0, 30.2, 29.8, 29.7, 29.7, 29.4, 29.4, 25.5, 24.1, 22.8, 14.3. HRMS (ESI) m/z : $[\text{M}+\text{H}]^+$ Calcd for $\text{C}_{41}\text{H}_{62}\text{N}$ 568.4882, found 568.4877.

10,10-Didodecyl-1,2-dimethyl-10H-indeno[1,2-g]quinolin-1-ium

iodide (5). The compound **4** (0.68 g, 1.2 mmol), MeI (0.85g, 6 mmol) and 2 mL acetonitrile were taken in a sealed tube and heated at 100 °C for 48 h. After the completion of the reaction the solvents were removed to give compound **5** as yellow gum which was used without further purification (0.767 g, 90%). ^1H NMR (200 MHz, CDCl_3) δ 8.87 (d, $J = 8.5$ Hz, 1H), 8.39 (s, 1H), 8.22 (s, 1H), 8.01 – 7.87 (m, 2H), 7.52 – 7.40 (m, 3H), 4.77 (s, 3H), 3.33 (s, 3H), 2.25 – 2.07 (m, 4H), 1.22 – 1.02 (m, 35H), 0.85 (t, $J = 6.4$ Hz, 6H), 0.63 – 0.44 (m, 4H). ^{13}C NMR (100 MHz, CDCl_3) δ 161.7, 159.0, 151.3, 145.4, 143.9, 140.1, 137.4, 130.6, 128.8, 128.1, 124.8, 123.6, 121.8, 119.4, 112.1, 57.0, 54.5, 41.6, 41.1, 32.0, 30.0, 29.71, 29.65, 29.4, 24.7, 24.2, 22.8, 14.2. HRMS (ESI) m/z : $[\text{M}]^+$ Calcd for $\text{C}_{42}\text{H}_{64}\text{N}^+$ 582.5033, found 582.5031.

General procedure for synthesizing ISQ dyes: Indenoquinolindinium iodide, **5** (1 equiv) and respective semi-squaric acid derivatives **P1**, or **P2** or **P3** (1.2 equiv) were dissolved in 10 mL of *n*-BuOH/PhMe (1:1) in a two-necked round bottom flask and fitted with Dean-Stark apparatus. Quinoline (1 mL) was added to the reaction mixture and refluxed for 24 h under argon atmosphere. The reaction mixture was cooled to room temperature, and the solvents were removed under reduced pressure. The residue was purified by column chromatography ($\text{MeOH}-\text{CH}_2\text{Cl}_2$) to afford the desired dye as dark green solid.

ISQ1: Started with **5** (0.2 g, 0.28 mmol) and **P1** (0.105 g, 0.34 mmol). Yield: 0.165 g, 67 %. m.p. 200–202 °C. ^1H NMR (400 MHz, CDCl_3) δ 9.57 (d, $J = 9.3$ Hz, 1H), 8.09 (d, $J = 8.4$ Hz, 1H), 8.03 (s, 1H), 7.98 – 7.87 (m, 2H), 7.85 – 7.72 (m, 1H), 7.54 (s, 1H), 7.44 – 7.34 (m, 3H), 6.87 (d, $J = 8.4$ Hz, 1H), 6.30 (s, 1H), 5.84 (s, 1H), 4.13 (s, 3H), 3.44 (s, 3H), 2.15 – 1.96 (m, 4H), 1.83 (s, 6H), 1.24 – 1.02 (m, 36H), 0.84 (t, $J = 6.9$ Hz, 6H), 0.65 – 0.49 (m, 4H). ^{13}C NMR (100 MHz, CDCl_3) δ 184.7, 181.8, 180.8, 170.5, 168.1, 165.4, 156.9, 153.7, 150.6, 148.1, 141.6, 139.8, 138.9, 136.8, 131.3, 128.8, 127.6, 125.7, 125.6, 124.0, 123.3, 123.2, 120.7, 119.2, 109.7, 107.3, 96.0, 87.8, 56.2, 47.5, 41.1, 37.8, 32.00, 30.4, 30.1, 29.7, 29.6, 29.4, 29.4, 27.6, 24.0, 22.8, 14.2. HRMS (ESI) m/z : $[\text{M}]^+$ Calcd for $\text{C}_{59}\text{H}_{76}\text{N}_2\text{O}_4$ 876.5805, found 876.5793.

ISQ2: Started with **5** (0.2 g, 0.28 mmol) and **P2** (0.101 g, 0.34 mmol). Yield: 0.121 g, 50 %. m.p. 180–182 °C. ^1H NMR (500 MHz, CDCl_3) δ 9.54 (d, $J = 9.1$ Hz, 1H), 8.70 (s, 1H), 8.19 (d, $J = 11.0$ Hz, 2H), 7.93 (d, $J = 8.0$ Hz, 1H), 7.87 (d, $J = 12.9$ Hz, 2H), 7.77 (d, $J = 4.4$ Hz, 1H), 7.49 (s, 1H), 7.38 (d, $J = 6.1$ Hz, 3H), 7.27 (s, 1H), 6.25 (s, 1H), 5.89 (s, 1H), 4.08 (s, 3H), 3.55 (s, 3H), 2.10 (s, 6H), 2.06 – 1.97 (m, 4H), 1.23 – 1.11 (m, 24H), 1.06 – 1.01 (m, 12H), 0.84 (t, $J = 7.1$ Hz, 6H), 0.64 – 0.55 (m, 4H). ^{13}C NMR (126 MHz, CDCl_3) δ 184.9, 181.9, 179.0, 168.8, 168.1, 156.6, 153.2, 150.6, 139.9, 139.4, 139.0, 136.1, 133.7, 133.1, 131.4, 131.2, 129.7, 128.6, 127.6, 127.0, 125.7, 125.4, 124.9, 123.2, 122.4, 120.6, 119.1, 110.5, 109.5, 95.4, 86.8, 56.1, 49.9, 41.1, 37.6, 32.0, 30.5, 30.1, 29.7, 29.7, 29.4, 29.4, 27.1, 24.0, 22.8, 14.2. HRMS (ESI) m/z : $[\text{M}]^+$ Calcd for $\text{C}_{63}\text{H}_{78}\text{N}_2\text{O}_4$ 926.5962, found 926.5956.

ISQ3: Started with **5** (0.2 g, 0.28 mmol) and **P3** (0.124 g, 0.34 mmol). Yield: 0.16 g, 60%. m.p. 142–144 °C. ^1H NMR (400 MHz, $[\text{D}_6]\text{DMSO}/\text{CDCl}_3$ (1:1)) δ 9.29 (d, $J = 9.3$ Hz, 1H), 9.05 (d, $J = 9.5$ Hz, 1H), 8.01 (s, 1H), 7.97 (s, 2H), 7.82 (d, $J = 9.4$ Hz, 1H), 7.75 (d, $J = 4.5$ Hz, 1H), 7.69 (s, 1H), 7.41 (d, $J = 8.9$ Hz, 1H), 7.37 – 7.33 (m, 2H), 7.32 – 7.29 (m, 2H), 5.84 (s, 1H), 5.57 (s, 1H), 3.97 (s, 3H), 3.64 (s, 3H), 2.08 – 1.96 (m, 4H), 1.17 – 1.05 (m, 24H), 1.00 – 0.95 (m, 12H), 0.79 (t, $J = 6.8$ Hz, 6H), 0.52

– 0.45 (m, 4H). ^{13}C NMR (100 MHz, $\text{DMSO}-d_6/\text{CDCl}_3$ (1:1)) δ 176.5, 170.8, 170.2, 156.1, 151.8, 150.5, 149.1, 143.6, 140.2, 139.2, 138.5, 135.2, 132.0, 131.3, 129.9, 129.5, 128.3, 127.5, 126.7, 125.0, 124.0, 123.1, 120.5, 119.1, 114.7, 110.3, 98.9, 94.5, 93.7, 79.2, 56.0, 37.5, 36.1, 31.8, 29.7, 29.5, 29.4, 29.2, 29.1, 23.8, 22.6, 14.3. HRMS (ESI) m/z : $[\text{M}]^+$ Calcd for $\text{C}_{58}\text{H}_{72}\text{N}_2\text{O}_4$ 860.5492, found 860.5474.

Acknowledgments

This work is financially supported by the Council of Scientific and Industrial Research (CSIR) Network Project NWP0054 (CSIR-TAPSUN), and SERB-EMR/2016/007114, India. R.B. thanks CSIR, New Delhi for research fellowships. J.N. thanks Dr. Kothandam Krishnamoorthy, Polymer Science Engineering Division, CSIR-National Chemical Laboratory, Pune, India, for his support, help with device fabrication and characterization. Authors also thank Mr. Ananthan Alagumalai for help with making a precursor.

Keywords: unsymmetrical squaraine dyes, Indenoquinolindine, H- and J-type aggregation, dye-sensitized solar cells, NIR active dyes, CDCA

- [1] a) A. Hagfeldt, G. Boschloo, L. Sun, L. Kloo, H. Pettersson, *Chem. Rev.* **2010**, *110*, 6595–6663; b) M. Grätzel, *J. Photochem. Photobiol. C Photochem. Rev.* **2003**, *4*, 145–153.
- [2] a) B. E. Hardin, H. J. Snaith, M. D. McGehee, *Nat. Photonics* **2012**, *6*, 162–169; b) J. Wu, Z. Lan, J. Lin, M. Huang, Y. Huang, L. Fan, G. Luo, *Chem. Rev.* **2015**, *115*, 2136–2173; c) S. Thomas, T. G. Deepak, G. S. Anjusree, T. A. Arun, S. V. Nair, A. S. Nair, *J. Mater. Chem. A* **2014**, *2*, 4474–4490; d) M.-E. Yeoh, K.-Y. Chan, *Int. J. Energy Res.* **2017**, *41*, 2446–2467; e) J. Gong, K. Sumathy, Q. Qiao, Z. Zhou, *Renew. Sustain. Energy Rev.* **2017**, *68*, 234–246; f) M. Freitag, J. Teuscher, Y. Saygili, X. Zhang, F. Giordano, P. Liska, J. Hua, S. M. Zakeeruddin, J.-E. Moser, M. Grätzel, A. Hagfeldt, *Nat. Photonics* **2017**, *11*, 372–378; g) P. Pinipthak, A. Kulkarni, H.-W. Chen, M. Ikegami, T. Miyasaka, *Bull. Chem. Soc. Jpn.* **2018**, *91*, 754–760; h) H. Shimogawa, M. Endo, T. Taniguchi, Y. Nakaïke, M. Kawaraya, H. Segawa, Y. Murata, A. Wakamiya, *Bull. Chem. Soc. Jpn.* **2017**, *90*, 441–450.
- [3] a) B. O'Regan, M. Grätzel, *Nature* **1991**, *353*, 737–740; b) A. S. Polo, M. K. Itokazu, N. Y. Murakami Iha, *Coord. Chem. Rev.* **2004**, *248*, 1343–1361; c) C.-Y. Chen, M. Wang, J.-Y. Li, N. Pootrakulchote, L. Alibabaei, C. Ngoc-le, J.-D. Decoppet, J.-H. Tsai, C. Grätzel, C.-G. Wu, S. M. Zakeeruddin, M. Grätzel, *ACS Nano* **2009**, *3*, 3103–3109.
- [4] a) L.-L. Li, E. W.-G. Diau, *Chem. Soc. Rev.* **2012**, *42*, 291–304; b) S. Mathew, A. Yella, P. Gao, R. Humphry-Baker, B. F. E. Curchod, N. Ashari-Astani, I. Tavernelli, U. Rothlisberger, M. K. Nazeeruddin, M. Grätzel, *Nat. Chem.* **2014**, *6*, 242–247; c) M. Urbani, M. Grätzel, M. K. Nazeeruddin, T. Torres, *Chem. Rev.* **2014**, *114*, 12330–12396; d) T. Higashino, H. Imahori, *Dalton Trans.* **2014**, *44*, 448–463.
- [5] a) A. Mishra, M. K. R. Fischer, P. Bäuerle, *Angew. Chem. Int. Ed.* **2009**, *48*, 2474–2499; b) M. Liang, J. Chen, *Chem. Soc. Rev.* **2013**, *42*, 3453–3488; c) Z.-S. Huang, H. Meier, D. Cao, *J. Mater. Chem. C* **2016**, *4*, 2404–2426.
- [6] a) M. Liang, J. Chen, *Chem. Soc. Rev.* **2013**, *42*, 3453–3488; b) A. Mahmood, *Sol. Energy* **2016**, *123*, 127–144; c) Y. Wu, W.-H. Zhu, S. M. Zakeeruddin, M. Grätzel, *ACS Appl. Mater. Interfaces* **2015**, *7*, 9307–9318; d) Y. Wu, W. Zhu, *Chem. Soc. Rev.* **2013**, *42*, 2039–2058.
- [7] a) W. Zeng, Y. Cao, Y. Bai, Y. Wang, Y. Shi, M. Zhang, F. Wang, C. Pan, P. Wang, *Chem. Mater.* **2010**, *22*, 1915–1925; b) N. Zhou, K. Prabakaran, B. Lee, S. H. Chang, B. Harutyunyan, P. Guo, M. R. Butler, A. Timalina, M. J. Bedzyk, M. A. Ratner, S. Vegiraju, S. Yau, C.-G. Wu, R. P. H. Chang, A. Facchetti, M.-C. Chen, T. J. Marks, *J. Am. Chem. Soc.* **2015**, *137*, 4414–4423; c) Y. Ezhumalai, B. Lee, M.-S. Fan, B. Harutyunyan, K. Prabakaran, C.-P. Lee, S. H. Chang, J.-S. Ni, S. Vegiraju, P. Priyanka, J.-W. Wu, C.-W. Liu, S. Yau, J. T. Lin, C.-

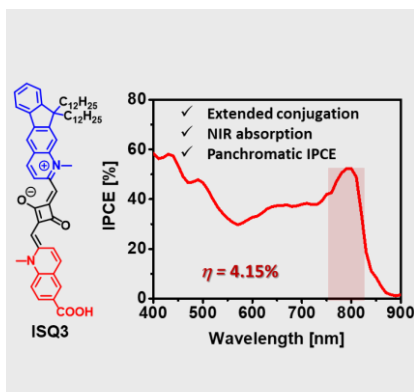
- G. Wu, M. J. Bedzyk, R. P. H. Chang, M.-C. Chen, K.-C. Ho, T. J. Marks, *J. Mater. Chem. A* **2017**, *5*, 12310–12321.
- [8] a) Z. Yao, M. Zhang, H. Wu, L. Yang, R. Li, P. Wang, *J. Am. Chem. Soc.* **2015**, *137*, 3799–3802; b) Z. Yao, M. Zhang, R. Li, L. Yang, Y. Qiao, P. Wang, *Angew. Chem. Int. Ed.* **2015**, *54*, 5994–5998; c) Y. Ren, D. Sun, Y. Cao, H. N. Tsoo, Y. Yuan, S. M. Zakeeruddin, P. Wang, M. Grätzel, *J. Am. Chem. Soc.* **2018**, *140*, 2405–2408.
- [9] K. Kakiage, Y. Aoyama, T. Yano, K. Oya, J. Fujisawa, M. Hanaya, *Chem. Commun.* **2015**, *51*, 15894–15897.
- [10] S. Zhang, X. Yang, Y. Numata, L. Han, *Energy Environ. Sci.* **2013**, *6*, 1443.
- [11] a) C. Qin, W.-Y. Wong, L. Han, *Chem. - Asian J.* **2013**, *8*, 1706–1719; b) P. Brogdon, H. Cheema, J. H. Delcamp, *ChemSusChem* **2018**, *11*, 86–103; c) L. Martín-Gomis, F. Fernández-Lázaro, A. Sastre-Santos, *J. Mater. Chem. A* **2014**, *2*, 15672–15682; d) M.-E. Ragoussi, M. Ince, T. Torres, *Eur. J. Org. Chem.* **2013**, *2013*, 6475–6489.
- [12] a) A. Ajayaghosh, *Acc. Chem. Res.* **2005**, *38*, 449–459; b) S. Sreejith, P. Carol, P. Chithra, A. Ajayaghosh, *J. Mater. Chem.* **2008**, *18*, 264–274.
- [13] a) K. Y. Law, *Chem. Rev.* **1993**, *93*, 449–486; b) S. Luo, E. Zhang, Y. Su, T. Cheng, C. Shi, *Biomaterials* **2011**, *32*, 7127–7138; c) V. J. Pansare, S. Hejazi, W. J. Faenza, R. K. Prud'homme, *Chem. Mater.* **2012**, *24*, 812–827; d) J. O. Escobedo, O. Rusin, S. Lim, R. M. Strongin, *Curr. Opin. Chem. Biol.* **2010**, *14*, 64–70.
- [14] a) P. Chithra, R. Varghese, K. P. Divya, A. Ajayaghosh, *Chem. - Asian J.* **2008**, *3*, 1365–1373; b) P. Anees, S. Sreejith, A. Ajayaghosh, *J. Am. Chem. Soc.* **2014**, *136*, 13233–13239; c) P. Anees, K. V. Sudheesh, P. Jayamurthy, A. R. Chandrika, R. V. Omkumar, A. Ajayaghosh, *Chem. Sci.* **2016**, *7*, 6808–6814; d) Philips Divya S., Ghosh Samrat, Sudheesh Karivachery V., Suresh Cherumuttathu H., Ajayaghosh Ayyappanpillai, *Chem. - Eur. J.* **2017**, *23*, 17973–17980.
- [15] a) C. W. Dirk, W. C. Herndon, F. Cervantes-Lee, H. Selnau, S. Martinez, P. Kalamegham, A. Tan, G. Campos, M. Velez, *J. Am. Chem. Soc.* **1995**, *117*, 2214–2225; b) C. Prabhakar, K. Bhanuprakash, V. J. Rao, M. Balamuralikrishna, D. N. Rao, *J. Phys. Chem. C* **2010**, *114*, 6077–6089.
- [16] a) D. Ramaiah, I. Eckert, K. T. Arun, L. Weidenfeller, B. Epe, *Photochem. Photobiol.* **2002**, *76*, 672–677; b) A. Yuan, J. Wu, X. Tang, L. Zhao, F. Xu, Y. Hu, *J. Pharm. Sci.* **2013**, *102*, 6–28.
- [17] a) C. Qin, W.-Y. Wong, L. Han, *Chem. - Asian J.* **2013**, *8*, 1706–1719; b) G. Chen, H. Sasabe, T. Igarashi, Z. Hong, J. Kido, *J. Mater. Chem. A* **2015**, *3*, 14517–14534.
- [18] Y. Shi, R. B. M. Hill, J.-H. Yum, A. Dualeh, S. Barlow, M. Grätzel, S. R. Marder, M. K. Nazeeruddin, *Angew. Chem. Int. Ed.* **2011**, *50*, 6619–6621.
- [19] R. Bisht, M. F. M. K., A. K. Singh, J. Nithyanandhan, *J. Org. Chem.* **2017**, *82*, 1920–1930.
- [20] S. Paek, H. Choi, C. Kim, N. Cho, S. So, K. Song, M. K. Nazeeruddin, J. Ko, *Chem. Commun.* **2011**, *47*, 2874–2876.
- [21] a) T. Maeda, S. Nitta, H. Nakao, S. Yagi, H. Nakazumi, *J. Phys. Chem. C* **2014**, *118*, 16618–16625; b) T. Maeda, S. Nitta, Y. Sano, S. Tanaka, S. Yagi, H. Nakazumi, *Dyes Pigments* **2015**, *122*, 160–167; c) T. Maeda, N. Shima, T. Tsukamoto, S. Yagi, H. Nakazumi, *Synth. Met.* **2011**, *161*, 2481–2487; d) K. Funabiki, H. Mase, Y. Saito, A. Otsuka, A. Hibino, N. Tanaka, H. Miura, Y. Himori, T. Yoshida, Y. Kubota, M. Matsui, *Org. Lett.* **2012**, *14*, 1246–1249.
- [22] J.-Y. Li, C.-Y. Chen, W.-C. Ho, S.-H. Chen, C.-G. Wu, *Org. Lett.* **2012**, *14*, 5420–5423.
- [23] S. Kuster, F. Sauvage, M. K. Nazeeruddin, M. Grätzel, F. A. Nüesch, T. Geiger, *Dyes Pigments* **2010**, *87*, 30–38.
- [24] T. Maeda, Y. Hamamura, K. Miyanaga, N. Shima, S. Yagi, H. Nakazumi, *Org. Lett.* **2011**, *13*, 5994–5997.
- [25] T. Maeda, S. Arikawa, H. Nakao, S. Yagi, H. Nakazumi, *New J. Chem.* **2013**, *37*, 701–708.
- [26] L. Zhang, J. M. Cole, *J. Mater. Chem. A* **2017**, *5*, 19541–19559.
- [27] G. de Miguel, M. Ziótek, M. Zitnan, J. A. Organero, S. S. Pandey, S. Hayase, A. Douhal, *J. Phys. Chem. C* **2012**, *116*, 9379–9389.
- [28] a) M. W. Kryman, J. N. Nasca, D. F. Watson, M. R. Detty, *Langmuir* **2016**, *32*, 1521–1532; b) M. Ziótek, J. Karolczak, M. Zalas, Y. Hao, H. Tian, A. Douhal, *J. Phys. Chem. C* **2014**, *118*, 194–205.
- [29] a) H.-P. Lu, C.-Y. Tsai, W.-N. Yen, C.-P. Hsieh, C.-W. Lee, C.-Y. Yeh, E. W.-G. Diau, *J. Phys. Chem. C* **2009**, *113*, 20990–20997; b) T. Takeshita, T. Umeda, M. Hara, *J. Photochem. Photobiol. Chem.* **2017**, *333*, 87–91; c) J. H. Delcamp, Y. Shi, J.-H. Yum, T. Sajoto, E. Dell'Orto, S. Barlow, M. K. Nazeeruddin, S. R. Marder, M. Grätzel, *Chem. - Eur. J.* **2013**, *19*, 1819–1827; d) F. M. Jradi, X. Kang, D. O'Neill, G. Pajares, Y. A. Getmanenko, P. Szymanski, T. C. Parker, M. A. El-Sayed, S. R. Marder, *Chem. Mater.* **2015**, *27*, 2480–2487.
- [30] J. Mei, Z. Bao, *Chem. Mater.* **2014**, *26*, 604–615.
- [31] A. Alagumalai, M. F. M. K., P. Vellimalai, M. C. Sil, J. Nithyanandhan, *ACS Appl. Mater. Interfaces* **2016**, *8*, 35353–35367.
- [32] a) Z. Yan, S. Guang, X. Su, H. Xu, *J. Phys. Chem. C* **2012**, *116*, 8894–8900; b) K. Jyothish, K. T. Arun, D. Ramaiah, *Org. Lett.* **2004**, *6*, 3965–3968.
- [33] K. Hara, Z.-S. Wang, T. Sato, A. Furube, R. Katoh, H. Sugihara, Y. Dan-oh, C. Kasada, A. Shinpo, S. Suga, *J. Phys. Chem. B* **2005**, *109*, 15476–15482.
- [34] S.-L. Li, K.-J. Jiang, K.-F. Shao, L.-M. Yang, *Chem. Commun.* **2006**, *0*, 2792–2794.
- [35] M. J. Frisch et al., *Gaussian 09*; Gaussian, Inc.: Wallingford, CT, USA, 2009. (Complete Reference Is Provided in Supporting Information).
- [36] T. Marinado, K. Nonomura, J. Nissfolk, M. K. Karlsson, D. P. Hagberg, L. Sun, S. Mori, A. Hagfeldt, *Langmuir* **2010**, *26*, 2592–2598.
- [37] a) J. Bisquert, D. Cahen, G. Hodes, S. Rühle, A. Zaban, *J. Phys. Chem. B* **2004**, *108*, 8106–8118; b) E. Ronca, M. Pastore, L. Belpassi, F. Tarantelli, F. D. Angelis, *Energy Environ. Sci.* **2012**, *6*, 183–193.

Entry for the Table of Contents (Please choose one layout)

Layout 1:

FULL PAPER

Three indenoquinaldine based unsymmetrical squaraine dyes were synthesized for dye-sensitized solar cells. The dye ISQ3 exhibited strong absorption in NIR region, panchromatic IPCE and efficiency up to 4.15 %.



Rajesh Bisht, Munavvar Fairoos Mele Kavungathodi, and Jayaraj Nithyanandhan*

Page No. – Page No.

Indenoquinaldine Based Unsymmetrical Squaraine Dyes for Near-Infrared Absorption: Investigating the Steric and Electronic Effects in Dye-sensitized Solar Cells